coatings

MDPI

Article

Silicon Dioxide Thin Films Deposited Using Oxide Targets: Results of Atomistic Simulation

F. V. Grigoriev [1,2,*], V. B. Sulimov [1,2] and A. V. Tikhonravov [1,2]

[1] Research Computing Center, M.V. Lomonosov Moscow State University, 119234 Moscow, Russia; vs@dimonta.com (V.B.S.); tikh@srcc.msu.ru (A.V.T.)
[2] Moscow Center for Fundamental and Applied Mathematics, 119234 Moscow, Russia
* Correspondence: fedor.grigoriev@gmail.com

Abstract: An atomistic simulation of silicon dioxide thin films deposited using oxide targets is performed. The influence of the oxide target on the deposition process is taken into account by introducing O=Si=O molecules into the flow of particles moving from the target to the substrate. The fraction of these molecules varied from 0 to 50%. It was found that the presence of O=Si=O molecules leads to film densification during a normal deposition. With a low-energy deposition, the increase in density was twice as high as with a high-energy deposition. The absolute value of the compressive stress increased with an increasing fraction of O=Si=O molecules in the flow of deposited particles at a normal, high-energy deposition. The influence of O=Si=O molecules on the structure of the glancing angle deposited films depends on the deposition angle.

Keywords: thin films; dielectric targets; molecular dynamics; silicon dioxide films

check for updates

Citation: Grigoriev, F.V.; Sulimov, V.B.; Tikhonravov, A.V. Silicon Dioxide Thin Films Deposited Using Oxide Targets: Results of Atomistic Simulation. *Coatings* **2024**, *14*, 258. https://doi.org/10.3390/coatings14030258

Academic Editor: Victor J. Rico

Received: 12 January 2024
Revised: 14 February 2024
Accepted: 19 February 2024
Published: 21 February 2024

Copyright: © 2024 by the authors. Licensee MDPI, Basel, Switzerland. This article is an open access article distributed under the terms and conditions of the Creative Commons Attribution (CC BY) license (https://creativecommons.org/licenses/by/4.0/).

1. Introduction

Optical coatings of various compositions are widely used in optic and optoelectronic devices for various purposes: high-quality linear filters for aerospace technologies [1], optical fiber sensors in medicine [2], photovoltaic cells [3], antireflective coatings [4], high-power lasers for fusion [5], and others [6]. Physical vapor deposition (PVD) is widely used to obtain multilayer optical coatings [6]. In the PVD method, a substance from a solid target is transferred into the gas phase by heating or sputtering; then, gas particles move through a vacuum chamber and condense on a substrate to form coating layers [7]. Both metal and oxide targets are used to produce optical coatings [6]. The metal targets are convenient from a technological point of view. At the same time, dielectric targets are also applied to produce transparent thin films.

Silicon dioxide is the main film-forming material with a low refractive index. SiO_2 films are produced using both metal [8–10] and oxide targets [11–15]. In the case of metal targets, individual atoms and metallic clusters pass into the gas phase from the target and are oxidized by the oxygen flow supplied to the vacuum chamber. Along with individual atoms, molecules consisting of metal and oxygen atoms can be emitted from dielectric targets. Differences in the composition of the flow of deposited particles can lead to differences in the structural and mechanical properties of growing films. This effect can be studied using atomistic modeling methods.

The composition and characteristics of emitted particles significantly depend on the parameters of the emission process [16]. For this reason, the simplest neutral molecule of the stoichiometric composition O=Si=O is chosen as an example of an atomistic cluster for modeling. It should be noted that this molecule is extremely reactive in favor of tetracoordinated Si clusters. Therefore, their presence in the particle flow is possible due to the essentially nonequilibrium nature of the emission process.

The simulation of the deposition process is performed using the previously developed molecular dynamics (MD)-based method [17,18]. Both high-energy and low-energy deposi-

tion processes are considered. The structural and mechanical parameters are calculated, including the density, density profiles, defects concentration, and mechanical stress values.

2. Methods

In previous works [17,18], the deposition of SiO_2 films was simulated assuming that only Si atoms are emitted from the target into the gas phase. These atoms interact with oxygen and form new layers of film on the surface of the substrate. In this work, the possibility of emitting the triatomic O=Si=O molecules from the target is taken into account. Thus, at the beginning of each deposition step, these molecules are placed at the top of the simulation window, along with silicon and oxygen atoms.

The initial coordinates of the atoms are chosen randomly, as are the coordinates of the Si atom of the O=Si=O molecules. The orientation of the molecules is also chosen randomly. The fraction of O=Si=O molecules in the flow of deposited particles is determined as follows:

$$f = N(SiO_2)/(N(Si) + N(SiO_2)), \quad (1)$$

where $N(SiO_2)$ and $N(Si)$ are the number of introduced O=Si=O molecules and Si atoms. The DESIL empirical force field [17] is used to calculate the energy of interatomic interactions:

$$U_{ij} = q_i q_j / r_{ij} + A_{ij}/r_{ij}^{12} - B_{ij}/r_{ij}^{6} \quad (2)$$

where $q_{i(j)}$ is the charge of the $i(j)$-th atom, $q_O = -0.65e$, $q_{Si} = 1.3e$, A_{ij}, and B_{ij}, are parameters of the Lennard-Jones potential for the van der Waals interaction, r_{ij} is the interatomic distance, $A_{SiO} = 4.6 \times 10^{-8}$ kJ·(nm)^{12}/mol, $A_{SiSi} = A_{OO} = 1.5 \times 10^{-6}$ kJ·(nm)^{12}/mol, $B_{SiO} = 4.2 \times 10^{-3}$ kJ·(nm)^{6}/mol, and $B_{SiSi} = B_{OO} = 5 \times 10^{-5}$ kJ·(nm)^{6}/mol. For silicon and oxygen atoms in O=Si=O, the DESIL force field is also used. This empirical force field is parameterized so as to reproduce experimental parameters of fused silica, including the density, Si–O bond length, nearest O–O and Si–Si distances ([18], Table 1), tetrahedron structural unit ([18], Figure 7), and some others.

The deposition simulation is organized as a step-by-step procedure [17] and begins with the preparation of a cluster of substrates on which the film grows. Each step of the deposition modeling includes the following points:

1. Adding O=Si=O molecules, Si, and O atoms in a stoichiometric ratio of 1:2 to the upper part of the simulation box;
2. MD modeling of the movement of these particles to the substrate and the formation of a structure on the surface of the substrate and previously deposited film layers;
3. Removing particles reflected from the film surface from the simulation box;
4. Increasing the vertical size of the simulation box by 0.01 nm to compensate for the increase in the thickness of the growing film.

The number of steps depends on the film thickness, and as a rule, reaches several thousand. Examples of the final structures are shown in Figure 1.

The values of the initial velocities correspond to the deposited atoms kinetic energies. To simulate high- and low-energy depositions, the energy values of silicon atoms are chosen to be 10 eV and 0.1 eV, respectively. The first value corresponds to the ion beam sputtering of the target [19] (high-energy method); the second value corresponds to the thermal emission of the target [6] (low-energy method). Also, these values are used earlier for the MD simulations of silicon dioxide [20,21] and titanium dioxide films [22]. The energy of individual oxygen atoms is 0.1 eV. The energy of the oxygen atoms in the O=Si=O molecules is equal to the energy of the silicon atoms.

The MD simulation step is equal to 0.5 fs, and the duration of one deposition step is equal to 10 ps. This time is sufficient for the deposited atoms to reach the film surface and transfer excess kinetic energy to the film atoms [23]. The total length of the MD trajectory depends on the final thickness of the film and reaches 25 ns, which corresponds to 2500 deposition steps. The maximum number of deposited atoms in the clusters is

4.5×10^6. The *NVT* (constant number of particles, volume, and temperature) ensemble with the periodic boundary conditions is used at every deposition step. All simulations are performed at room temperature, T = 300 K, using the Berendsen thermostat [24]. For the MD part of the modeling, the GROMACS package [25] is used. For the visual analysis of deposited clusters, the Visual Molecular Dynamic (VMD) package is applied [26]. The simulation is carried out using equipment at the shared research facilities of high-performance computing resources at Lomonosov Moscow State University [27].

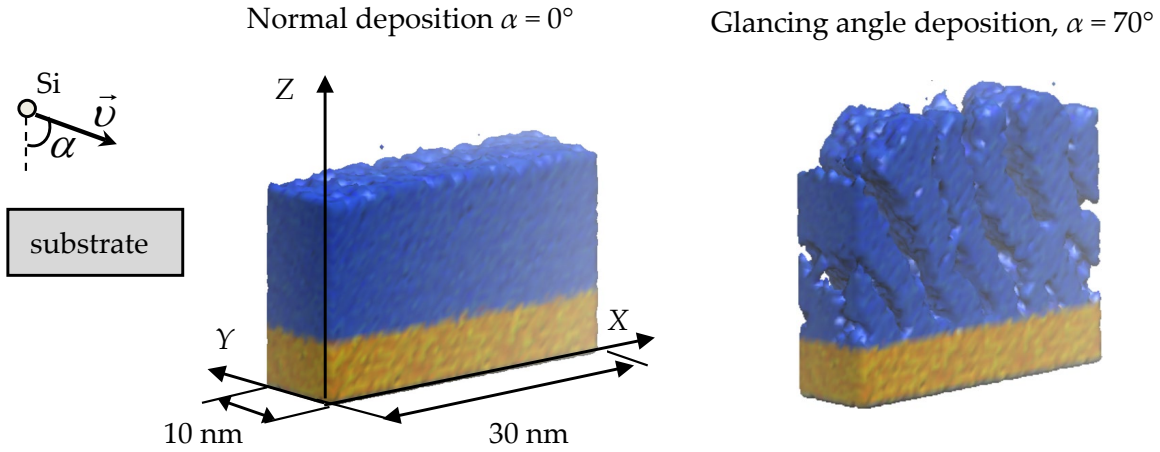

Figure 1. Geometries of the clusters deposited at different deposition angles α.

3. Results and Discussion

The parameters of the O=Si=O molecule are shown in Table 1. The quantum chemistry calculations are performed using GAMESS US program [28] at the HF/6-31G* level. This level is sufficient to reproduce the ground state geometry of a simple molecule. The classical calculations are performed using the DESIL force field, which is used in the present work to simulate the deposition process. As can be seen from the results of Table 1, the classical method reproduces the linear geometry of the O=Si=O molecule and slightly overestimates the length of the double bonds between the oxygen and silicon atoms. At the same time, the DESIL force field overestimates the stability of the O=Si=O molecule: the difference in the formation energies of a Si_2O_4 molecule and two O=Si=O molecules is −291 kJ/mol (DESIL) and −447 kJ/mol (HF/6-31G*). This means that DESIL underestimates the realized energy during the transition of Si atoms from the double bond configuration in O=Si=O molecules to the tetrahedral configuration in films.

Table 1. Parameters of O=Si=O molecule, calculated using quantum chemistry (QC) method and DESIL force field (FF).

Method	R(Si-O), nm	α(O-Si-O), grad	Charge
QC	0.149	180	0
FF	0.155	180	0

The energy and angular distribution of the sputtered particles, as well as their composition, essentially depend on the sputtering parameters, such as the angle between the flow of bombarding ions and the substrate [16], the surface binding energy [29], and others. For this reason, in this work, the fraction of molecules in the flow of the deposited particles varies widely. It is assumed in the simulation that the distance between the target and substrate is much more than the substrate dimension. Due to this assumption, the directions of the initial velocities of deposited atoms are considered to be the same. In the following text, we will call the angles of the selected directions the deposition angles.

The results of modeling normally deposited films, when the deposition angle α is equal to zero, are shown in Figures 2 and 3. The sharp change in the density (about h = 5 nm) is associated with the transition from the substrate to the film. The deposition temperature is 300 K, which corresponds to a cold substrate. The density profiles of growing films are obtained for high- and low-energy depositions when the fraction of O=Si=O molecules in the flow of incident atoms varies from 0 to 40%. In the case of the high-energy deposition (E = 10 eV), an increase in f leads to an increase in the film density. At the same time, the addition of O=Si=O molecules to the flow of incident atoms slightly changes the shapes of the density profiles.

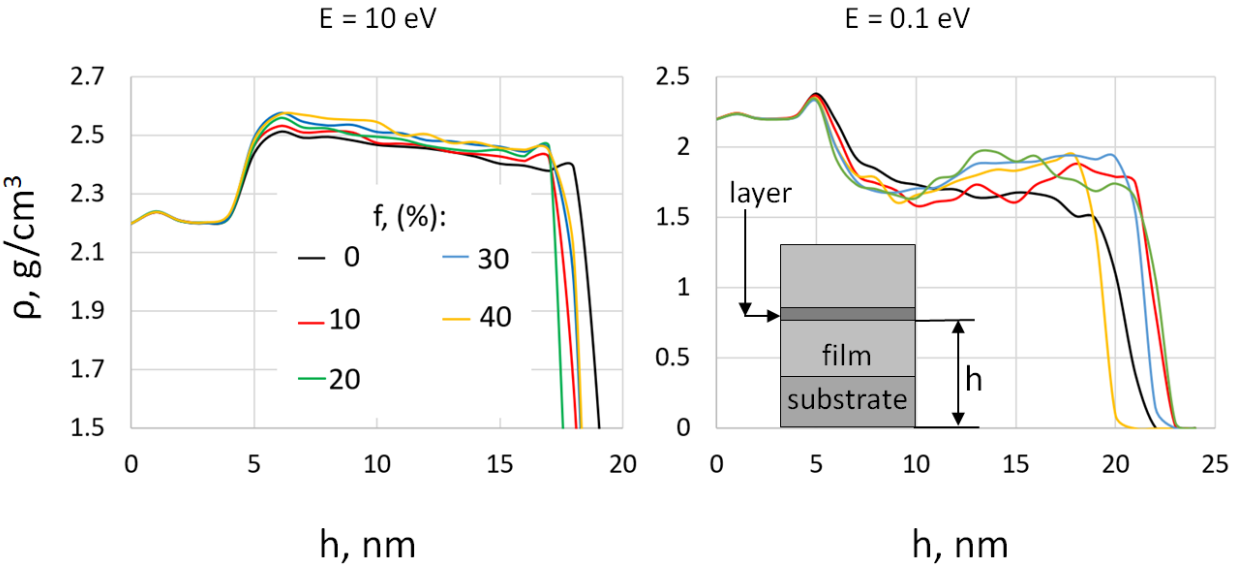

Figure 2. Density profiles of deposited silicon dioxide films. h—distance from the layer of thickness of 1 nm to the substrate, f—fraction of O=Si=O molecules in the flow of deposited particles, and E—particle energy.

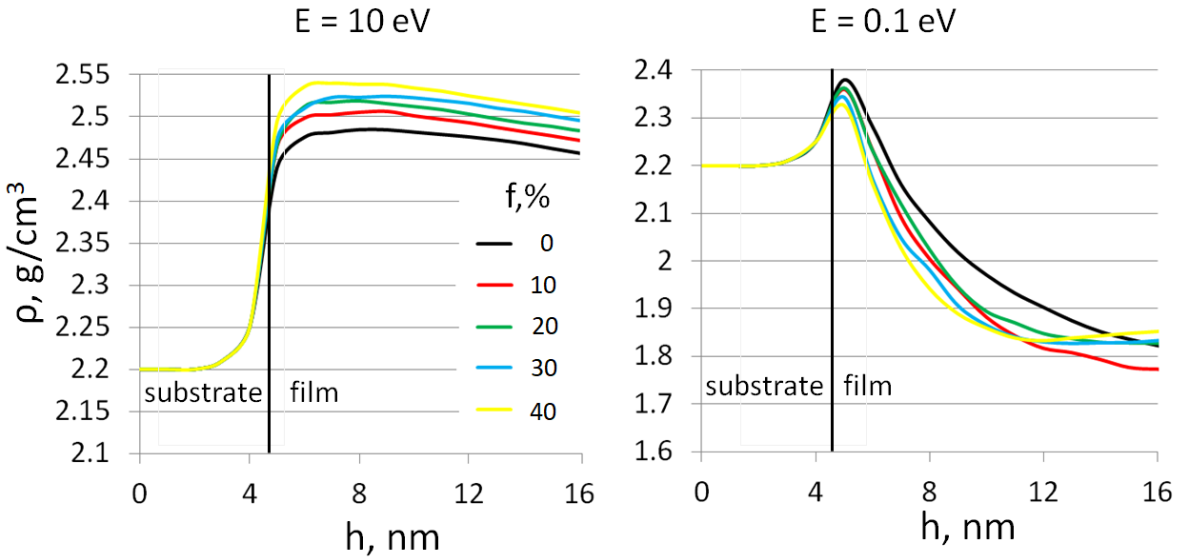

Figure 3. Dependence of the film's density of the film's thickness h. f is the fraction of the O=Si=O molecules in the flow of the deposited particles, and E is the energy of the particles. The vertical line indicates the substrate boundary (h = 5 nm). The substrate is not included in the film density (h > 5 nm).

For low-energy sputtering (E = 0.1 eV), the dependence of the density profiles on the value of f is more complex than for E = 10 eV. The difference between the profiles increases

with an increasing *h* value. The density of the transition layers between the film and the substrate decreases with an increasing fraction of O=Si=O molecules, but with a further increase in *h*, the density increases. In general, the introduction of molecules into the flow of incident atoms leads to film densification, as in the high-energy deposition. The increase in density reaches approximately 0.5 g/cm^3, (see plots in the range from 15 to 20 nm), which is twice the similar effect at E = 10 eV.

The dependence of the film density on its thickness is shown in Figure 3. The film density monotonically increases as *f* changes from 0 to 40%, but with an increasing *f* value, this effect weakens. The density of low-energy deposited films decreases with an increasing *h*. At *h* > 14–15 nm, the density of films deposited at *f* = 20–40% exceeds the density of films deposited without O=Si=O molecules in the flow of incoming atoms. This is explained by a noticeable increase in the density of sub-layers deposited with an increasing h (Figure 2).

For a more detailed study of the dependence of the film structure on the value of *f*, averaged values of the following structural parameters were calculated: the length of the Si–O bonds (0.164 nm), the Si–O–Si angle (145°), and the concentration of point defects such as undercoordinated oxygen (1%) and silicon (0.1%) atoms. These defects significantly affect the optical properties of transparent films, such as the laser damage threshold.

It was revealed that all these structural parameters weakly depend on the fraction of molecules in the flow of incident atoms during the high-energy deposition. This means that linear O=Si=O molecules in the film change their geometry and participate in the formation of structural SiO_4 tetrahedra (Figure 4).

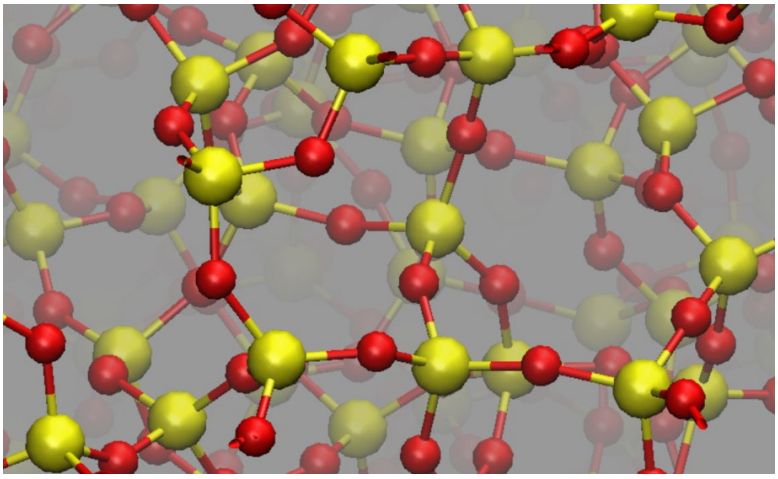

Figure 4. Fragment of the atomistic structure of a deposited film. The formation of structural tetrahedra is shown.

The observed increase in the film density is likely due to a change in the relative orientation of these tetrahedra. A similar result is obtained with low-energy sputtering, with one exception: the concentration of single-coordinated, non-bridging oxygen atoms increases by ten percent as *f* changes from 0 to 40%. This means that a small fraction of O=Si=O molecules retain non-bridging oxygen in the film.

Mechanical stresses arising in the film during the deposition process can significantly affect the properties of the film [6]. In this work, the main components of the stress tensor σ_{xx} and σ_{yy} in the plane of the substrate are calculated as follows [20]: after the deposition is complete, the final cluster is simulated in the NVT ensemble, the diagonal components of the pressure tensor p_{xx} and p_{yy} are averaged over MD trajectory, and then, σ_{xx} and σ_{yy} values are calculated as $\sigma_{xx(yy)} = -p_{xx(yy)}$. The stresses are calculated for a cluster with a thickness of *h* = 20 nm. The simulation is carried out at T = 300 K for 100 ps. This trajectory length is sufficient to eliminate stress fluctuations [20].

The results for the high-energy deposited film are presented in Table 2. The values of σ_{xx} and σ_{yy} are negative, $\sigma_{xx(yy)} = -|\sigma_{xx(yy)}|$, which corresponds to the compressive type

of stress. This is consistent with the results of MD stress calculations performed previously for SiO_2 films [20] and experimental data [30,31]. The absolute values of the stress tensor components increase with an increasing f value. This means that the introduction of O=Si=O molecules into the flow of incident atoms leads to an increase in stress in the growing film. This result can be explained as follows: Using larger particles to form a film reduces the flexibility of the growing structure to adapt to the external pressure. Therefore, the stress increases with the increasing proportion of O=Si=O molecules. The values of the stress tensor components in the low-energy deposited films are insignificant and change slightly with an increasing f.

Table 2. Main components of the stress tensor, σ_{xx} and σ_{yy} (MPa), where f is the fraction of the O=Si=O molecules in the flow of the deposited particles.

f, %	0	10	20	30	40	50
$\lvert \sigma_{xx} \rvert$	117	133	152	160	162	165
$\lvert \sigma_{yy} \rvert$	122	138	140	148	162	170

The change of the refractive index Δn due to the change in the film density $\Delta\rho$ is calculated using Gladstone–Dale equation [32] in the following form:

$$\Delta n = 0.21 \cdot \Delta\rho, \quad (3)$$

In the case of the high-energy deposition, the change in the density $\Delta\rho$ with varying values of f from 0 to 40% is approximately 0.05 g/cm^3 (Figure 3, left side, h = 16 nm). According to Equation (3), this corresponds to an increase in the refractive index by $\Delta n = 0.001$. With the low-energy deposition, the density changes from 1.77 g/cm^3 to 1.85 g/cm^3 with a change in f (Figure 3, right side, h = 16 nm), which corresponds to a change in the refractive index by $\Delta n = 0.017$.

The simulation of the deposition under large angles (glancing angle deposition, GLAD) is also carried out. GLAD films are characterized by a high porosity and anisotropy of the structure [19]. As can be seen in the plots in Figures 5 and 6, an increase in the deposition angle from $\alpha = 60°$ to $\alpha = 70°$ leads to a significant reduction in the film density. This result is consistent with the experiments [33] and results of previous simulations [34].

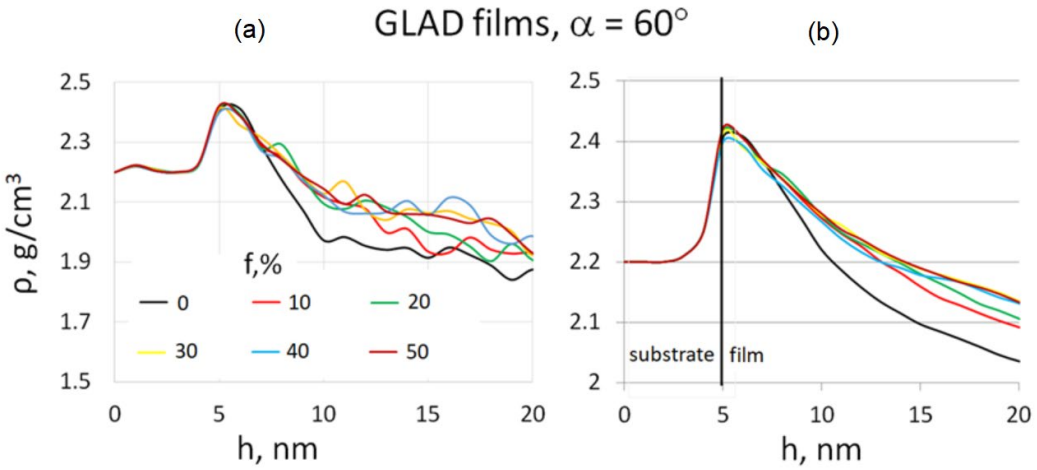

Figure 5. Density profiles (**a**) and dependence of the density on the film's thickness h (**b**). f is the fraction of the Si=O=Si molecules in the flow of the deposited particles, the energy of the deposited particles is E = 10 eV, and α is the deposition angle. The vertical line indicates the substrate boundary (h = 5 nm) (**b**). The substrate is not included in the film density (h > 5 nm).

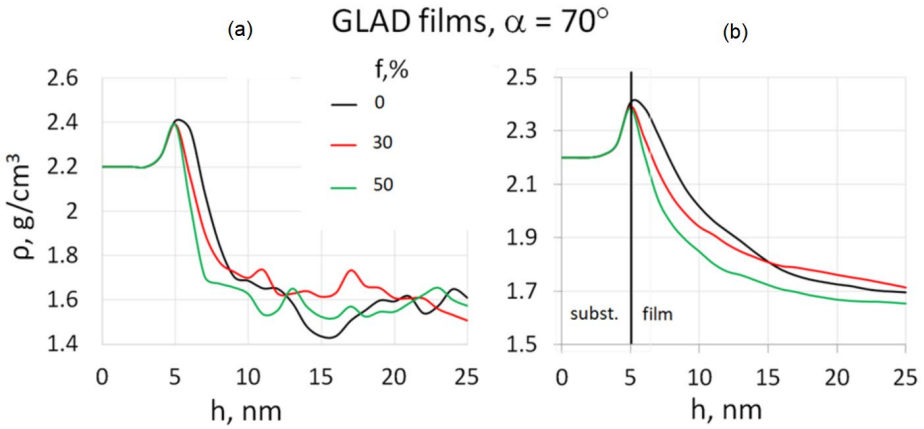

Figure 6. Density profiles (**a**) and dependence of the density on the film's thickness *h* (**b**). The designations are the same as in the caption to Figure 5.

In the case of $\alpha = 60^\circ$, the introduction of O=Si=O molecules into the flow of deposited atoms leads to an increase in the film density (Figure 5). The density profiles show that after the formation of a thin layer of increased density adjacent to the substrate, the density of the layers decreases significantly with the increasing coordinate *h* of the layers (Figure 5a). This behavior is observed for all values of *f*. The increase in the layer density depends on *f* and can reach 0.2 g/cm^3. The film density increases by approximately 0.05 g/cm^3 at $f = 10\%$ (h = 20 nm). A further increase in *f* to 50% results in an increase in the density by approximately the same amount (Figure 5b). In general, the film density at $\alpha = 60^\circ$ changes approximately in the same way as during the normal deposition.

In the case of $\alpha = 70^\circ$, an increase in the fraction of O=Si=O molecules leads to multidirectional changes in the density profiles and the dependence of the film's density on its thickness (Figure 6). The change in the layer density caused by an increase in the *f* value can reach 0.2 g/cm^3 (Figure 6a). This change can be either positive or negative. In the transition region between the substrate and the film, when *h* changes from 5 nm to 10 nm, an increase in *f* leads to a decrease in the density. If $h > 10$ nm, the density change fluctuates with an increase in the value of *f*.

The difference in the film density, $\rho(f = 30\%) - \rho(f = 0)$, is initially negative, but becomes positive when *h* exceeds 15 nm (Figure 6a). In the case of $f = 50\%$, the film density is lower than in the case of $f = 0$ for all values of the film thickness. Thus, the film density changes nonmonotonically with an increasing *f*. This result is attributed to large-scale structure fluctuations at the initial stage of growth of the GLAD film deposited at $\alpha = 70^\circ$ [35].

4. Conclusions

The MD modeling of silicon dioxide films deposited using a dielectric target, which is a source of deposited particles, was carried out. For the first time in a full-atomistic MD simulation, the flow of deposited particles included not only individual silicon and oxygen atoms, but also O=Si=O molecules.

If the flow of deposited particles moves perpendicular to the substrate, then the introduction of O=Si=O molecules into the flow leads to the densification of the film during both high-energy and low-energy depositions. With the low-energy deposition (E(Si) = 0.1 eV), the increase in the density can reach approximately 0.5 g/cm^3, which is twice as high as the similar effect with the high-energy deposition (E = 10 eV). This densification is associated with a change in the mutual orientation of the SiO_4 structural tetrahedra, since the length of the Si–O bonds and the Si–O–Si angle change slightly. The change in the refractive index due to film densification can reach 0.025 for low-energy deposited films.

The main components of the stress tensor were calculated using a previously developed approach. In the case of the high-energy deposition, the stress was compressive,

which is consistent with experimental data and modeling results known from the literature. The absolute values of the stress tensor components increased with increasing fractions of O=Si=O molecules in the flow of deposited particles. The stresses in low-energy sputtered films were insignificant.

Glancing angle deposition (GLAD) simulations were also performed. At a deposition angle of $\alpha = 60^\circ$, the film density changed approximately in the same way as with a normal deposition. In the case of $\alpha = 70^\circ$, an increase in the fraction of O=Si=O molecules led to multidirectional changes in the dependence of the film density on its thickness.

In general, the simulation results are consistent with the experimental data and simulation results known from literature. The features of the structure and properties of films caused by the presence of molecules in the flow of deposited particles are discussed in the work.

Author Contributions: Conceptualization, A.V.T.; Methodology, F.V.G.; Software, V.B.S.; Data curation, V.B.S.; Writing—original draft, F.V.G.; Writing—review & editing, A.V.T.; Supervision, A.V.T. All authors have read and agreed to the published version of the manuscript.

Funding: This research was funded by the Russian Science Foundation (grant No. 23-11-00047). The part of the work related to the organization and optimization of the supercomputer calculations was funded by the Ministry of Education and Science of the Russian Federation as part of the program of the Moscow Center for Fundamental and Applied Mathematics under the agreement No. 075-15-2022-284.

Institutional Review Board Statement: Not applicable.

Informed Consent Statement: Not applicable.

Data Availability Statement: Data are contained within the article.

Conflicts of Interest: The authors declare no conflict of interest.

References

1. Tang, H.; Gao, J.; Zhang, J.; Wang, X.; Fu, X. Preparation and Spectrum Characterization of a High Quality Linear Variable Filter. *Coatings* **2018**, *8*, 308. [CrossRef]
2. Qu, W.; Chen, Y.; Ma, C.; Peng, D.; Bai, X.; Zhao, J.; Liu, S.; Luo, L. Application of Optical Fiber Sensing Technology and Coating Technology in Blood Component Detection and Monitoring. *Coatings* **2024**, *14*, 173. [CrossRef]
3. Barranco, A.; Borras, A.; Gonzalez-Elipe, A.R.; Palmero, A. Perspectives on Oblique Angle Deposition of Thin Films: From Fundamentals to Devices. *Prog. Mater. Sci.* **2016**, *76*, 59–153. [CrossRef]
4. Raut, H.K.; Ganesh, V.A.; Nair, A.S.; Ramakrishna, S. Anti-Reflective Coatings: A Critical, in-Depth Review. *Energy Environ. Sci.* **2011**, *4*, 3779–3804. [CrossRef]
5. Manenkov, A.A. Fundamental Mechanisms of Laser-Induced Damage in Optical Materials: Today's State of Understanding and Problems. *Opt. Eng.* **2014**, *53*, 010901. [CrossRef]
6. Angela Piegari, F.F. (Ed.) *Optical Thin Films and Coatings*; Elsevier: Amsterdam, The Netherlands, 2018.
7. Greene, J.E. Review Article: Tracing the Recorded History of Thin-Film Sputter Deposition: From the 1800s to 2017. *J. Vac. Sci. Technol. A* **2017**, *35*, 05C204. [CrossRef]
8. Mateev, M.; Lautenschläger, T.; Spemann, D.; Finzel, A.; Gerlach, J.W.; Frost, F.; Bundesmann, C. Systematic Investigation of the Reactive Ion Beam Sputter Deposition Process of SiO_2. *Eur. Phys. J. B* **2018**, *91*, 45. [CrossRef]
9. Tolenis, T.; Grinevičiūtė, L.; Smalakys, L.; Ščiuka, M.; Drazdys, R.; Mažulė, L.; Buzelis, R.; Melninkaitis, A. Next Generation Highly Resistant Mirrors Featuring All-Silica Layers. *Sci. Rep.* **2017**, *7*, 10898. [CrossRef]
10. Bernstein, J.; Gerlach, J.W.; Finzel, A.; Bundesmann, C. Ion Beam Sputter Deposition of SiO_2 thin Films Using Oxygen Ions. *Eur. Phys. J. B* **2022**, *95*, 39. [CrossRef]
11. He, X.; Wu, J.; Li, X.; Gao, X.; Zhao, L.; Wu, L. Synthesis and Properties of Silicon Dioxide Films Prepared by Pulsed Laser Deposition Using Ceramic SiO_2 Target. *Appl. Surf. Sci.* **2009**, *256*, 231–234. [CrossRef]
12. Bhatt, V.; Chandra, S. Silicon Dioxide Films by RF Sputtering for Microelectronic and MEMS Applications. *J. Micromech. Microeng.* **2007**, *17*, 1066. [CrossRef]
13. Fogarassy, E.; Slaoui, A.; Fuchs, C.; Stoquert, J.P. Deposition of SiO_2 by Reactive Excimer Laser Ablation from a SiO Target. *Appl. Surf. Sci.* **1990**, *46*, 195–199. [CrossRef]
14. Telesh, E.V.; Dostanko, A.P.; Gurevich, O. V Stoichiometry of Silicon Dioxide Films Obtained by Ion-Beam Sputtering. *J. Appl. Spectrosc.* **2018**, *85*, 67–72. [CrossRef]
15. Ristau, D.; Gross, T. Ion Beam Sputter Coatings for Laser Technology. In Proceedings of the Optical Systems Design 2005, Jena, Germany, 13–15 September 2005; SPIE: Bellingham, WA, USA, 2005; Volume 5963, p. 596313.

16. Kim, D.-H.; Lee, G.-H.; Yup Lee, S.; Hyun Kim, D. Atomic Scale Simulation of Physical Sputtering of Silicon Oxide and Silicon Nitride Thin Films. *J. Cryst. Growth* **2006**, *286*, 71–77. [CrossRef]
17. Grigoriev, F.V.; Sulimov, A.V.; Kochikov, I.; Kondakova, O.A.; Sulimov, V.B.; Tikhonravov, A.V. High-Performance Atomistic Modeling of Optical Thin Films Deposited by Energetic Processes. *Int. J. High Perform. Comput. Appl.* **2014**, *29*, 184–192. [CrossRef]
18. Grigoriev, F.V.; Sulimov, A.V.; Katkova, E.V.; Kochikov, I.V.; Kondakova, O.A.; Sulimov, V.B.; Tikhonravov, A.V. Computational Experiments on Atomistic Modeling of Thin Film Deposition. *Appl. Opt.* **2017**, *56*, C87–C90. [CrossRef]
19. Hawkeye, M.M.; Brett, M.J. Glancing Angle Deposition: Fabrication, Properties, and Applications of Micro- and Nanostructured Thin Films. *J. Vac. Sci. Technol. A Vac. Surf. Film.* **2007**, *25*, 1317. [CrossRef]
20. Grigoriev, F.V.; Sulimov, V.B.; Tikhonravov, A.V. Atomistic Simulation of Stresses in Growing Silicon Dioxide Films. *Coatings* **2020**, *10*, 220. [CrossRef]
21. Taguchi, M.; Hamaguchi, S. MD Simulations of Amorphous SiO_2 Thin Film Formation in Reactive Sputtering Deposition Processes. *Thin Solid Films* **2007**, *515*, 4879–4882. [CrossRef]
22. Badorreck, H.; Steinecke, M.; Jensen, L.; Ristau, D.; Jupé, M.; Müller, J.; Tonneau, R.; Moskovkin, P.; Lucas, S.; Pflug, A.; et al. Correlation of Structural and Optical Properties Using Virtual Materials Analysis. *Opt. Express* **2019**, *27*, 22209–22225. [CrossRef]
23. Grigoriev, F.V.; Sulimov, A.V.; Katkova, E.V.; Kochikov, I.V.; Kondakova, O.A.; Sulimov, V.B.; Tikhonravov, A.V. Full-Atomistic Nanoscale Modeling of the Ion Beam Sputtering Deposition of SiO_2 Thin Films. *J. Non. Cryst. Solids* **2016**, *448*, 1–5. [CrossRef]
24. Berendsen, H.J.C.; Postma, J.P.M.; Van Gunsteren, W.F.; Dinola, A.; Haak, J.R. Molecular Dynamics with Coupling to an External Bath. *J. Chem. Phys.* **1984**, *81*, 3684–3690. [CrossRef]
25. Abraham, M.J.; Murtola, T.; Schulz, R.; Páll, S.; Smith, J.C.; Hess, B.; Lindahl, E. GROMACS: High Performance Molecular Simulations through Multi-Level Parallelism from Laptops to Supercomputers. *SoftwareX* **2015**, *1*, 19–25. [CrossRef]
26. Humphrey, W.; Dalke, A.; Schulten, K. VMD: Visual Molecular Dynamics. *J. Mol. Graph.* **1996**, *14*, 33–38. [CrossRef]
27. Voevodin, V.V.; Antonov, A.S.; Nikitenko, D.A.; Shvets, P.A.; Sobolev, S.I.; Sidorov, I.Y.; Stefanov, K.S.; Voevodin, V.V.; Zhumatiy, S.A. Supercomputer Lomonosov-2: Large Scale, Deep Monitoring and Fine Analytics for the User Community. *Supercomput. Front. Innov.* **2019**, *6*, 4–11.
28. Schmidt, M.W.; Baldridge, K.K.; Boatz, J.A.; Elbert, S.T.; Gordon, M.S.; Jensen, J.H.; Koseki, S.; Matsunaga, N.; Nguyen, K.A.; Su, S.; et al. General Atomic and Molecular Electronic Structure System. *J. Comput. Chem.* **1993**, *14*, 1347–1363. [CrossRef]
29. Hofsäss, H.; Zhang, K.; Mutzke, A. Simulation of Ion Beam Sputtering with SDTrimSP, TRIDYN and SRIM. *Appl. Surf. Sci.* **2014**, *310*, 134–141. [CrossRef]
30. Begou, T.; Lumeau, J. Accurate Analysis of Mechanical Stress in Dielectric Multilayers. *Opt. Lett.* **2017**, *42*, 3217–3220. [CrossRef]
31. Abadias, G.; Chason, E.; Keckes, J.; Sebastiani, M.; Thompson, G.B.; Barthel, E.; Doll, G.L.; Murray, C.E.; Stoessel, C.H.; Martinu, L. Review Article: Stress in Thin Films and Coatings: Current Status, Challenges, and Prospects. *J. Vac. Sci. Technol. A* **2018**, *36*, 20801. [CrossRef]
32. Vedam, K.; Limsuwan, P. Piezo- and Elasto-optic Properties of Liquids under High Pressure. II. Refractive Index vs Density. *J. Chem. Phys.* **1978**, *69*, 4772–4778. [CrossRef]
33. Melninkaitis, A.; Grinevičiūtė, L.; Abromavičius, G.; Mažulė, L.; Smalakys, L.; Pupka, E.; Ščiuka, M.; Buzelis, R.; Kičas, S. Next-Generation All-Silica Coatings for UV Applications. In Proceedings of the Laser-Induced Damage in Optical Materials 2017, Colorado, CO, USA, 24–27 September 2017; SPIE: Bellingham, WA, USA, 2017; Volume 10447.
34. Grigoriev, F.V.; Sulimov, V.B.; Tikhonravov, A.V. Atomistic Simulation of the Glancing Angle Deposition of SiO_2 Thin Films. *J. Non Cryst. Solids* **2019**, *512*, 98–102. [CrossRef]
35. Tait, R.N.; Smy, T.; Brett, M.J. Modelling and Characterization of Columnar Growth in Evaporated Films. *Thin Solid Films* **1993**, *226*, 196–201. [CrossRef]

Disclaimer/Publisher's Note: The statements, opinions and data contained in all publications are solely those of the individual author(s) and contributor(s) and not of MDPI and/or the editor(s). MDPI and/or the editor(s) disclaim responsibility for any injury to people or property resulting from any ideas, methods, instructions or products referred to in the content.